H.E.S.S.

FITS data

Data level 3, public test release 1
September 2018

H.E.S.S. Collaboration, H. Abdalla[1], A. Abramowski[2], F. Aharonian[3,4,5],
F. Ait Benkhali[3], E.O. Angüner[6], M. Arakawa[7], C. Arcaro[1], C. Armand[8], M. Arrieta[9],
M. Backes[10,1], M. Barnard[1], Y. Becherini[11], J. Becker Tjus[12], D. Berge[13], S. Bernhard[14],
K. Bernlöhr[3], R. Blackwell[15], M. Böttcher[1], C. Boisson[9], J. Bolmont[16], S. Bonnefoy[13],
P. Bordas[3], J. Bregeon[17], F. Brun[18], P. Brun[19], M. Bryan[20], M. Büchele[21], T. Bulik[22],
T. Bylund[11], M. Capasso[23], S. Caroff[24], A. Carosi[8], S. Casanova[25,3], M. Cerruti[16],
N. Chakraborty[3], S. Chandra[1], R.C.G. Chaves[17,26], A. Chen[27], S. Colafrancesco[27],
B. Condon[18], I.D. Davids[10], J. Decock[19], C. Deil[3], J. Devin[17], P. deWilt[15], L. Dirson[2],
A. Djannati-Ataï[28], A. Donath[3], L.O'C. Drury[4], J. Dyks[29], T. Edwards[3], K. Egberts[30],
G. Emery[16], J.-P. Ernenwein[6], S. Eschbach[21], S. Fegan[24], A. Fiasson[8], G. Fontaine[24],
S. Funk[21], M. Füßling[13], S. Gabici[28], Y.A. Gallant[17], T. Garrigoux[1], F. Gaté[8],
G. Giavitto[13], D. Glawion[31], J.F. Glicenstein[19], D. Gottschall[23], M.-H. Grondin[18],
J. Hahn[3], M. Haupt[13], G. Heinzelmann[2], G. Henri[32], G. Hermann[3], J.A. Hinton[3],
W. Hofmann[3], C. Hoischen[30], T. L. Holch[33], M. Holler[14], D. Horns[2], D. Huber[14],
H. Iwasaki[7], A. Jacholkowska[16], M. Jamrozy[34], D. Jankowsky[21], F. Jankowsky[31],
L. Jouvin[28], I. Jung-Richardt[21], M.A. Kastendieck[2], K. Katarzyński[35], M. Katsuragawa[36],
U. Katz[21], D. Kerszberg[16], D. Khangulyan[7], B. Khélifi[28], J. King[3], S. Klepser[13],
W. Kluźniak[29], Nu. Komin[27], K. Kosack[19], S. Krakau[12], M. Kraus[21], P.P. Krüger[1],
G. Lamanna[8], J. Lau[15], J. Lefaucheur[9], A. Lemière[28], M. Lemoine-Goumard[18],
J.-P. Lenain[16], E. Leser[30], T. Lohse[33], M. Lorentz[19], R. Liu[3], R. López-Coto[3], I. Lypova[13],
D. Malyshev[23], V. Marandon[3], A. Marcowith[17], C. Mariaud[24], R. Marx[3], G. Maurin[8],
P.J. Meintjes[37], A.M.W. Mitchell[3], R. Moderski[29], M. Mohamed[31], L. Mohrmann[21],
E. Moulin[19], T. Murach[13], S. Nakashima[36], M. de Naurois[24], H. Ndiyavala [1],
F. Niederwanger[14], J. Niemiec[25], L. Oakes[33], P. O'Brien[38], H. Odaka[36], S. Ohm[13],
M. Ostrowski[34], I. Oya[13], M. Padovani[17], M. Panter[3], R.D. Parsons[3], C. Perennes[16],
P.-O. Petrucci[32], B. Peyaud[19], Q. Piel[8], S. Pita[28], V. Poireau[8], D.A. Prokhorov[27],
H. Prokoph[13], G. Pühlhofer[23], M. Punch[28,11], A. Quirrenbach[31], S. Raab[21], R. Rauth[14],
A. Reimer[14], O. Reimer[14], M. Renaud[17], R. de los Reyes[3], F. Rieger[3,39], L. Rinchiuso[19],
C. Romoli[3], G. Rowell[15], B. Rudak[29], E. Ruiz-Velasco[3], V. Sahakian[40,5], S. Saito[7],
D.A. Sanchez[8], A. Santangelo[23], M. Sasaki[21], R. Schlickeiser[12], F. Schüssler[19],
A. Schulz[13], U. Schwanke[33], S. Schwemmer[31], M. Seglar-Arroyo[19], A.S. Seyffert[1],
N. Shafi[27], I. Shilon[21], K. Shiningayamwe[10], R. Simoni[20], H. Sol[9], F. Spanier[1],
A. Specovius[21], M. Spir-Jacob[28], Ł. Stawarz[34], R. Steenkamp[10], C. Stegmann[30,13],
C. Steppa[30], I. Sushch[1], T. Takahashi[36], J.-P. Tavernet[16], T. Tavernier[19], A.M. Taylor[13],
R. Terrier[28], L. Tibaldo[3], D. Tiziani[21], M. Tluczykont[2], C. Trichard[6], M. Tsirou[17],
N. Tsuji[7], R. Tuffs[3], Y. Uchiyama[7], D.J. van der Walt[1], C. van Eldik[21], C. van Rensburg[1],
B. van Soelen[37], G. Vasileiadis[17], J. Veh[21], C. Venter[1], A. Viana[3,41], P. Vincent[16],
J. Vink[20], F. Voisin[15], H.J. Völk[3], T. Vuillaume[8], Z. Wadiasingh[1], S.J. Wagner[31],
P. Wagner[33], R.M. Wagner[42], R. White[3], A. Wierzcholska[25], A. Wörnlein[21], R. Yang[3],
D. Zaborov[24], M. Zacharias[1], R. Zanin[3], A.A. Zdziarski[29], A. Zech[9], F. Zefi[24],
A. Ziegler[21], J. Zorn[3], and N. Żywucka[34]

[1]Centre for Space Research, North-West University, Potchefstroom 2520, South Africa
[2]Universität Hamburg, Institut für Experimentalphysik, Luruper Chaussee 149, D 22761 Hamburg, Germany
[3]Max-Planck-Institut für Kernphysik, P.O. Box 103980, D 69029 Heidelberg, Germany
[4]Dublin Institute for Advanced Studies, 31 Fitzwilliam Place, Dublin 2, Ireland
[5]National Academy of Sciences of the Republic of Armenia, Marshall Baghramian Avenue, 24, 0019
Yerevan, Republic of Armenia
[6]Aix Marseille Université, CNRS/IN2P3, CPPM, Marseille, France

[7]Department of Physics, Rikkyo University, 3-34-1 Nishi-Ikebukuro, Toshima-ku, Tokyo 171-8501, Japan

[8]Laboratoire d'Annecy de Physique des Particules, Univ. Grenoble Alpes, Univ. Savoie Mont Blanc, CNRS, LAPP, 74000 Annecy, France

[9]LUTH, Observatoire de Paris, PSL Research University, CNRS, Université Paris Diderot, 5 Place Jules Janssen, 92190 Meudon, France

[10]University of Namibia, Department of Physics, Private Bag 13301, Windhoek, Namibia

[11]Department of Physics and Electrical Engineering, Linnaeus University, 351 95 Växjö, Sweden

[12]Institut für Theoretische Physik, Lehrstuhl IV: Weltraum und Astrophysik, Ruhr-Universität Bochum, D 44780 Bochum, Germany

[13]DESY, D-15738 Zeuthen, Germany

[14]Institut für Astro- und Teilchenphysik, Leopold-Franzens-Universität Innsbruck, A-6020 Innsbruck, Austria

[15]School of Physical Sciences, University of Adelaide, Adelaide 5005, Australia

[16]Sorbonne Université, Université Paris Diderot, Sorbonne Paris Cité, CNRS/IN2P3, Laboratoire de Physique Nucléaire et de Hautes Energies, LPNHE, 4 Place Jussieu, F-75252 Paris, France

[17]Laboratoire Univers et Particules de Montpellier, Université Montpellier, CNRS/IN2P3, CC 72, Place Eugène Bataillon, F-34095 Montpellier Cedex 5, France

[18]Université Bordeaux, CNRS/IN2P3, Centre d'Études Nucléaires de Bordeaux Gradignan, 33175 Gradignan, France

[19]IRFU, CEA, Université Paris-Saclay, F-91191 Gif-sur-Yvette, France

[20]GRAPPA, Anton Pannekoek Institute for Astronomy, University of Amsterdam, Science Park 904, 1098 XH Amsterdam, The Netherlands

[21]Friedrich-Alexander-Universität Erlangen-Nürnberg, Erlangen Centre for Astroparticle Physics, Erwin-Rommel-Str. 1, D 91058 Erlangen, Germany

[22]Astronomical Observatory, The University of Warsaw, Al. Ujazdowskie 4, 00-478 Warsaw, Poland

[23]Institut für Astronomie und Astrophysik, Universität Tübingen, Sand 1, D 72076 Tübingen, Germany

[24]Laboratoire Leprince-Ringuet, Ecole Polytechnique, CNRS/IN2P3, F-91128 Palaiseau, France

[25]Instytut Fizyki Jądrowej PAN, ul. Radzikowskiego 152, 31-342 Kraków, Poland

[26]Funded by EU FP7 Marie Curie, grant agreement No. PIEF-GA-2012-332350

[27]School of Physics, University of the Witwatersrand, 1 Jan Smuts Avenue, Braamfontein, Johannesburg, 2050 South Africa

[28]APC, AstroParticule et Cosmologie, Université Paris Diderot, CNRS/IN2P3, CEA/Irfu, Observatoire de Paris, Sorbonne Paris Cité, 10, rue Alice Domon et Léonie Duquet, 75205 Paris Cedex 13, France

[29]Nicolaus Copernicus Astronomical Center, Polish Academy of Sciences, ul. Bartycka 18, 00-716 Warsaw, Poland

[30]Institut für Physik und Astronomie, Universität Potsdam, Karl-Liebknecht-Strasse 24/25, D 14476 Potsdam, Germany

[31]Landessternwarte, Universität Heidelberg, Königstuhl, D 69117 Heidelberg, Germany

[32]Univ. Grenoble Alpes, CNRS, IPAG, F-38000 Grenoble, France

[33]Institut für Physik, Humboldt-Universität zu Berlin, Newtonstr. 15, D 12489 Berlin, Germany

[34]Obserwatorium Astronomiczne, Uniwersytet Jagielloński, ul. Orla 171, 30-244 Kraków, Poland

[35]Centre for Astronomy, Faculty of Physics, Astronomy and Informatics, Nicolaus Copernicus University, Grudziadzka 5, 87-100 Torun, Poland

[36]Japan Aerpspace Exploration Agency (JAXA), Institute of Space and Astronautical Science (ISAS), 3-1-1 Yoshinodai, Chuo-ku, Sagamihara, Kanagawa 229-8510, Japan

[37]Department of Physics, University of the Free State, PO Box 339, Bloemfontein 9300, South Africa

[38]Department of Physics and Astronomy, The University of Leicester, University Road, Leicester, LE1 7RH, United Kingdom

[39]Heisenberg Fellow (DFG), ITA Universität Heidelberg, Germany

[40]Yerevan Physics Institute, 2 Alikhanian Brothers St., 375036 Yerevan, Armenia

[41]Now at Instituto de Física de São Carlos, Universidade de São Paulo, Av. Trabalhador São-carlense, 400 - CEP 13566-590, São Carlos, SP, Brazil

[42]Oskar Klein Centre, Department of Physics, Stockholm University, Albanova University Center, SE-10691 Stockholm, Sweden

Date: September 18, 2018

Abstract

The High Energy Stereoscopic System (H.E.S.S.) is an array of ground-based imaging atmospheric Cherenkov telescopes in Namibia. For the first time, the H.E.S.S. collaboration is releasing a small dataset of event lists and instrument response information. This is a test data release, with the motivation to support the ongoing efforts to define open high-level data models and associated formats, as well as open-source science tools for gamma-ray astronomy. The data are in FITS format. Open-source science tools that support this format exist already.

The release data consists of 27.9 hours in total of observations of the Crab nebula, PKS $2155-304$, MSH $15-52$ and RX J1713.7-3946 taken with the H.E.S.S. 1 array. Most data are from 2004, the PKS $2155-304$ data are from 2006 and 2008. In addition, 20.7 hours of off observations of empty fields of view are included. The targets and observations were chosen to be suitable for common analysis use cases, including point-like and extended sources for spectral and morphology measurements, as well as a variable source (PKS $2155-304$) and the off dataset for background studies. The total size of the files in this data release is 42.8 MB.

This is a very small subset of the thousands of hours of H.E.S.S. 1 observations taken since 2004. The quality of this dataset, and measurements derived from this data, does not reflect the state of the art for H.E.S.S. publications, e.g. the event reconstruction and gamma-hadron separation method used here is a very basic one.

Webpage: `https://www.mpi-hd.mpg.de/hfm/HESS/pages/dl3-dr1/`

Questions or comments: contact.hess@hess-experiment.eu.

This data release was prepared by the H.E.S.S. FITS data task group. Members (current and former) include: Christoph Deil, Lars Mohrmann, Johannes King, Catherine Boisson, Axel Donath, Julien Lefaucheur, Bruno Khélifi, Léa Jouvin, Régis Terrier, Alexander Ziegler, Domenico Tiziani, Christopher Sobel, Karl Kosack, Michael Mayer and Anneli Schulz.

This data is released under the terms of use stated in the README.txt file, which is included here verbatim:

Contents

1. Introduction

1.1 H.E.S.S.

The High Energy Stereoscopic System (H.E.S.S.)[1] is an array of imaging air Cherenkov telescopes (IACTs) situated in the Khomas Highland, Namibia, at 1800 meter above sea level. Since 2004, four telescopes (H.E.S.S. Phase I) with mirror surfaces of ~ 100 m^2 have been detecting air showers produced by γ rays in the 100 GeV to 100 TeV energy band. This array forms a square of 120 m side length. It has a field of view of 5 deg in diameter, a spatial resolution of ~ 0.1 deg and an energy resolution of $\sim 15\%$ [1]. In September 2012, a fifth telescope placed in the middle of the original square was inaugurated, initiating H.E.S.S. Phase II. It has a mirror surface of ~ 600 m^2 and lowers the energy threshold of H.E.S.S. to tens of GeV. The data in this release were taken mostly in 2004 (some in 2005-2008), all with the four H.E.S.S. 1 telescopes.

1.2 Context

Ground-based gamma-ray astronomy is a relatively new window on the cosmos. The existing ground-based IACTs like e.g. H.E.S.S., MAGIC and VERITAS, have been operating independently for the past decade, using proprietary data formats and codes. The Cherenkov Telescope Array (CTA), the next IACT instrument, will probe the non-thermal universe above 20 GeV up to a few 100 TeV with an unmatched sensitivity and angular resolution compared to the current IACT experiments. CTA will be the first ground-based gamma-ray telescope array operated as an open observatory with public observer access. This implies fundamentally different requirements for the data formats and software tools and a challenge on their implementation to make very high energy (VHE) gamma-ray astronomy as accessible as any other waveband.

The Flexible Image Transport System (FITS) has been used by astronomers as a data interchange and archiving format for decades ([2], `http://fits.gsfc.nasa.gov/`). Space missions in X-ray or high-energy astronomy also store the list of recorded events, containing information like their arrival direction, time and energy, in FITS file format[2]. This is not yet the case within the VHE

---

[1] `https://www.mpi-hd.mpg.de/hfm/HESS/`
[2] `https://heasarc.gsfc.nasa.gov/docs/heasarc/ofwg/ofwg_intro.html`

astronomy community, particularly among the international collaborations operating ground-based IACTs, due to the different culture regarding data and software distribution in the particle physics community compared to the astrophysics one.

With that in mind and following on the work in CTA to provide DL3 event lists and IRF information in FITS format ([3]), H.E.S.S. Collaboration members have written exporters for DL3 data from different reconstruction chains to FITS format for internal use. The current DL3 data model and format definition needs to be tested on observations, to judge whether it properly specifies all data necessary for high-level science analysis. Such an effort is thus a valuable test bench and input for discussion in view of CTA.

Agreeing on a common data format for files greatly simplifies mid-level (event energies, positions) and high-level (source position, morphology, spectrum) checks between the different chains, algorithms and open-source tools. This will also ease interoperability with other codes (e.g. to check results, combine results in one plot, . . .). Currently two open-source science tools packages are being designed for current IACT and CTA data analysis, Gammapy [4, 5] and ctools [6]. *Gammapy* is an in-development Astropy-affiliated package, which is mainly written in Python, and *ctools* is based on the GammaLib analysis framework, which is mainly written in C++. Both can read as input the format used for this H.E.S.S. data release.

The format specifications currently being developed can form the basis for prototyping for data producers (i.e. existing IACTs and simulated CTA data) and consumers (i.e. science tool codes). They are made accessible on Github[3], so that they are visible by all, not just CTA members. Such open specifications also provide a basis to discuss the proposed DL3 model and format with members of other IACT experiments, aiming towards a common standard how to archive, diffuse and consume DL3 data.

1.3 Aims

The goal of this high-level data release (event lists and IRFs for high-level science analysis) is to have real VHE data publicly available for software and analysis method testing, and not to release data for science analysis.

A small set of data taken on TeV sources is made available. This dataset is prepared to allow a larger community to get their hands on VHE data, and to give feedback on the format and open-source tools. This will allow to explore requirements for analysis software.

VHE astronomers will have the opportunity to explore their familiar data with the open-source science tools currently designed for analysis of astronomical gamma-ray data, and also with standard tools used in the analysis of data in other wavelengths (e.g. ftools, xspec, . . .). Astronomers, who have not yet worked in the field of VHE astronomy, will get a first view on the details of VHE data analysis while dealing with familiar format and tools.

This will also be beneficial for CTA, which can profit from the experience gained by this release.

---

[3]`https://github.com/open-gamma-ray-astro/gamma-astro-data-formats`

2. Dataset

2.1 Overview

The data released consist of 27.9 hours of observations of the Crab nebula, PKS 2155−304, MSH 15−52 and RX J1713.7−3946 taken with the H.E.S.S. 1 array. Most data are from 2004, the PKS 2155−304 data are from 2006 and 2008. In addition, 20.7 hours of off observations of empty fields of view are included. This is a very small subset of the thousands of hours of H.E.S.S. 1 observations taken since 2004. The targets and observations were chosen to be suitable for common analysis use cases, including point-like and extended sources for spectral and morphology measurements, as well as a variable source (PKS 2155−304) and the off dataset for background studies.

The data consist of so-called "runs", which are observations of usually 28 min duration (sometimes less) on a fixed RA/DEC position in the sky, identified by a unique observation identifier (`OBS_ID`). This release contains 105 runs in total: 60 runs observing a gamma-ray source and 45 off runs. There are 1,046,156 events (on average 9,963 per run), most of which are cosmic-ray air-shower background events.

A summary of all sources and observations is given in Tables 2.1, 2.2 and Figure 2.1. The complete run list (grouped by source) is given in Table A.2 on page 33 in Appendix A.2. Table 2.3 contains a summary of the available event statistics for each source, i.e. an estimate of the number of excess gamma-ray events and the background level.

The following sections give some information on each source, as well as a counts image and spectrum (stacked for all observations) illustrating the spatial and energy distribution of the events.

Source name	RA	DEC	Type	Size	H.E.S.S. publications
Crab nebula	83.63	22.01	PWN	Point-like	[1], [7]
PKS 2155−304	329.72	−30.23	AGN	Point-like	[8], [9], [10]
MSH 15−52	228.53	−59.16	PWN	Small	[11], [12]
RX J1713.7−3946	258.35	39.77	SNR	Large	[13], [14], [15]

Table 2.1: Sources included in this release. The H.E.S.S. publications are only given for reference, the datasets from these publications do not match the ones released here. The positions given here are from SIMBAD for the Crab nebula pulsar and the AGN for PKS 2155−304, the position of MSH 15−52 is the best-fit position from [11]; for RX J1713.7−3946 from [15].

Source Name	N_{runs}	Time (h)	Dates
Crab	4	1.9	2004-12-04 - 2004-12-08
PKS 2155-304 (flare)	15	7.0	2006-07-29 - 2006-07-30
PKS 2155-304 (steady)	6	2.8	2008-08-27 - 2008-08-28
MSH 15-52	20	9.1	2004-03-26 - 2004-04-19
RX J1713.7-3946	15	7.0	2004-04-17 - 2004-05-21
Off data	45	20.7	2004-04-14 - 2005-11-20

Table 2.2: Observation dataset summary. N_{runs} is the number of observations. The table gives the observation time in hours and the range of dates when the observations took place. Information on the available event statistics in these datasets is given in Table 2.3. A full list of observations is given in Table A.2.

Source name	θ	N^{all}	N^{on}	N^{on}_{γ}	N^{on}_{bkg}	S
Crab	0.3	30,129	1,549	1,084.0	465.0	33.0
PKS 2155-304 (flare)	0.3	141,715	24,164	21,549.9	2,614.1	197.0
PKS 2155-304 (steady)	0.3	36,888	1,115	380.8	734.2	11.4
MSH 15-52	0.3	227,830	5,963	1,459.5	4,503.5	18.2
RX J1713.7-3946	0.5	226,264	16,696	3,652.1	13,043.9	24.2

Table 2.3: Event summary statistics information for each data set. (See Table 2.2 for the definition of each data set, and Table 2.1 for the positions used for this measurement.) The number of events in the total data set for each source is given as N^{all} (no energy or field of view offset cut). Using circular aperture photometry and a simple ring background estimate, a source gamma-ray excess $N^{on}_{\gamma} = N^{on} - N^{on}_{bkg}$ and significance S estimate using equation (17) from Li & Ma [16] was obtained. The on-region size radius θ (in deg) is given in the table. The background ring was chosen with radius $0.4 - 0.7$ deg ($0.6 - 0.9$ deg for RX J1713.7−3946), no acceptance correction was applied.

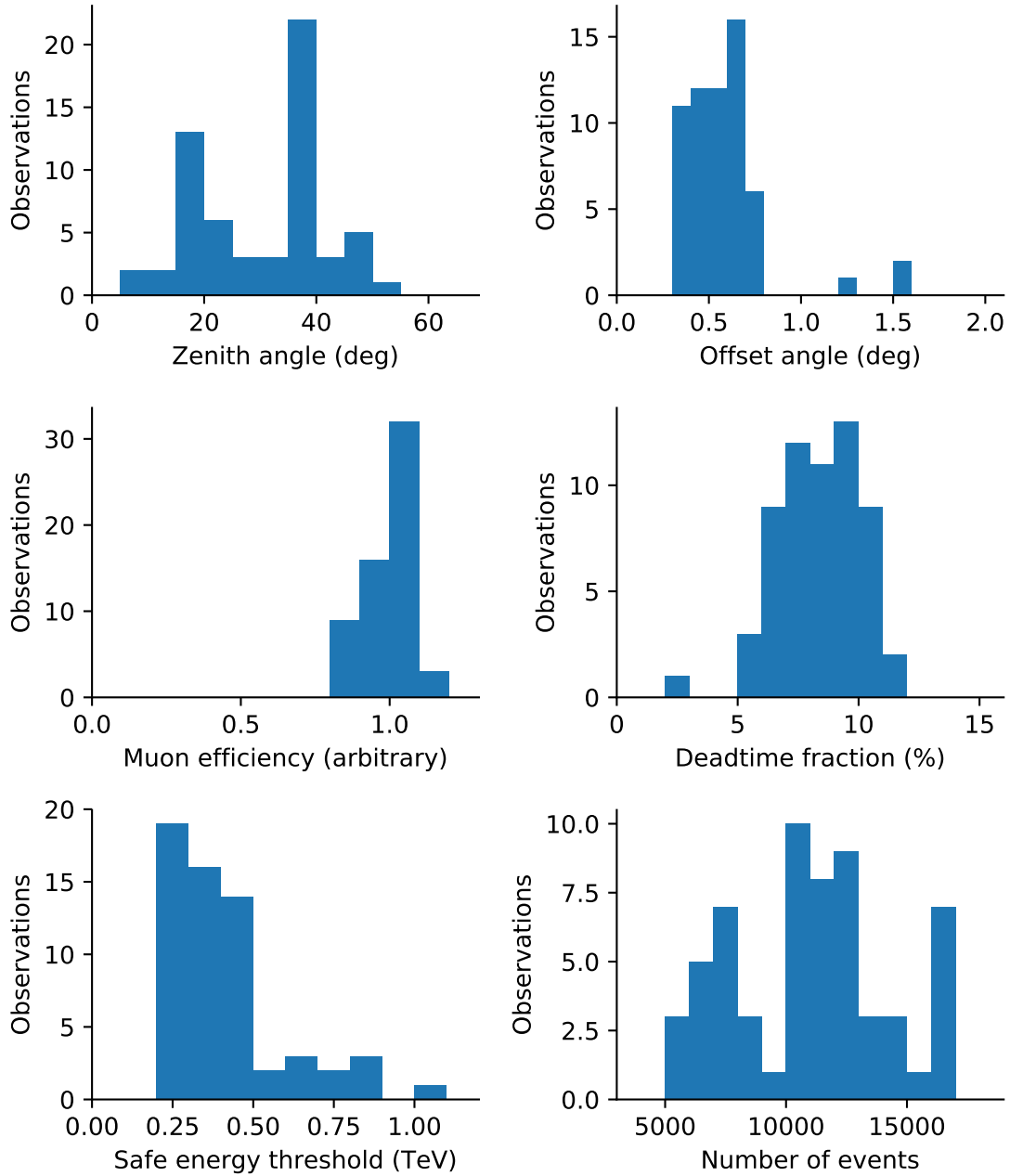Figure 2.1: Summary of parameters for the 60 observation runs in this data release. The parameters for the 45 off runs are not shown. Offset angle is the sky separation between the pointing position and the target. Muon efficiency is explained in Section 4.1.2, deadtime fraction in Section 3.3 and safe energy threshold in Section 4.2.2. The number of events is for all energies and the whole field of view.

2.2 Crab nebula

The Crab nebula was the first VHE gamma-ray source detected and is one of the brightest in the VHE sky. Gamma-ray emission has been detected from the pulsar (dominating at GeV energies) and pulsar wind nebula (dominating at TeV energies). Variability was detected at GeV energies [17]. Recently, the extension of the TeV nebula was measured [7].

This data release contains 1.9 hours of observation (4 runs) of the Crab nebula. The observations were taken in 2004 and are a very small subset of the data used in the 2006 H.E.S.S. paper on the Crab nebula [1]. Two of the runs are taken with the telescope pointing with an offset of 0.5 deg from the source position, two runs with an offset of 1.5 deg. The data set is illustrated in Figure 2.2. It contains ~ 1000 gamma rays, with a significant signal from energy threshold at ~ 600 GeV up to ~ 10 TeV. The energy threshold for this source is high because the observations were taken at a high zenith angle (45-48 deg).

The Crab nebula was chosen for this data release because it is possibly the most well-known and studied gamma-ray source. There is no variability in this data set and the small size of the dataset and the low precision of the IRFs do not allow for a precision measurement as recently done for the extension in [7].
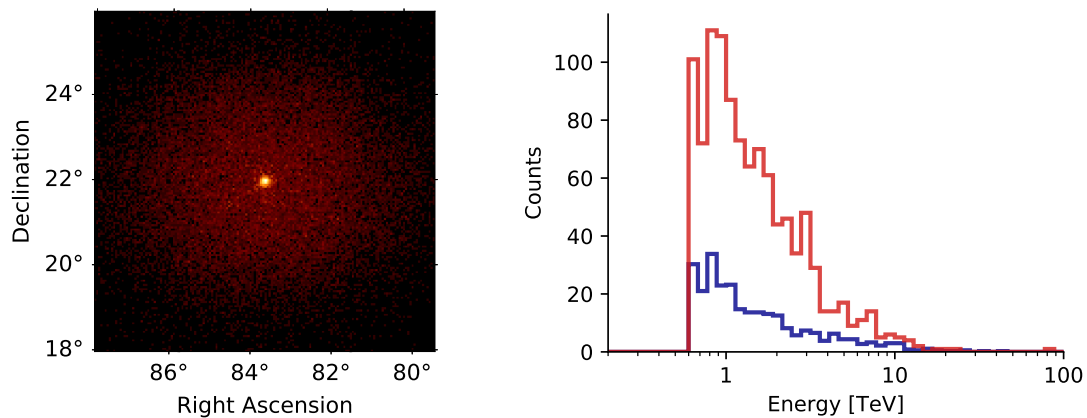

Figure 2.2: Crab nebula counts image (left) and counts spectrum (right) for a circular on region (total in red, background estimate using ring method in blue).

2.3 PKS 2155−304

Two different sets of data are presented for the extra-galactic source PKS 2155−304, an active galactic nucleus (AGN) with bright and highly variable TeV emission. The motivation to include these datasets in this data release was to have a variable source. It is point-like with a known position, i.e. studies of this source will focus on variability and spectrum.

The **PKS 2155−304 (flare)** data set (see Figure 2.3) contains 7.0 hours of observation (15 runs) from the nights of July 29 and 30, 2006 (around MJD 53946), when the source underwent a major gamma-ray outburst during its high-activity state of summer 2006. This H.E.S.S. dataset as well as simultaneous observations with the Chandra satellite were previously published in [8, 9, 10]. All data were taken at an offset of 0.5 deg, spanning a zenith angle range of 7-50 deg. The source was very bright and variable, the total excess in this dataset is $\sim 21,000$ gamma rays.

The **PKS 2155−304 (steady)** data set (see Figure 2.4) contains 2.8 hours of observation (6 runs) from 2008, taken at an offset of 0.5 deg and zenith angle of 23-37 deg, with an excess of ~ 400 gamma rays.

Figure 2.3: PKS 2155−304 (flare) counts image (left) and counts spectrum (right) for a circular on region (total in red, background estimate using ring method in blue).
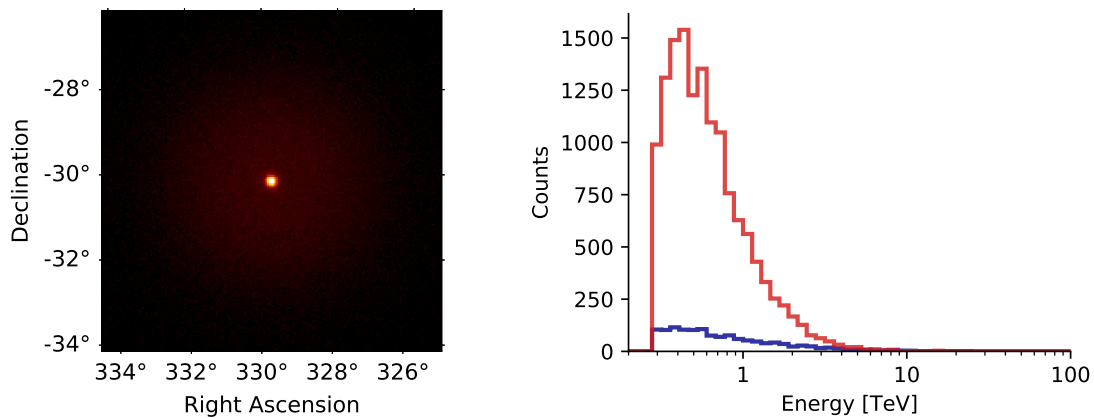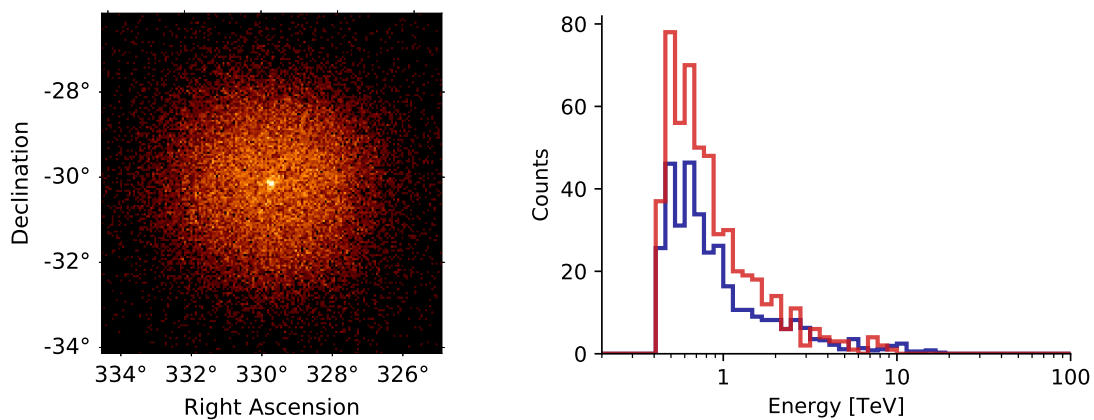

Figure 2.4: PKS 2155−304 (steady) counts image (left) and counts spectrum (right) for a circular on region (total in red, background estimate using ring method in blue).

2.4   MSH 15−52

The supernova remnant MSH 15−52 is a complex object with an unusual morphology. It contains the pulsar PSR B1509−58 and an extended, asymmetric pulsar wind nebula that has been observed at X-ray energies by ROSAT, as well as more recently at high angular resolution by Chandra. At TeV energies, H.E.S.S. has also observed a small, but clearly extended and elongated source [11, 12]. The TeV emission is thought to come from the pulsar wind nebula, rather than from the pulsar or the supernova remnant.

This data release contains 9.1 hours of observation (20 runs) of MSH 15−52 from 2004, a small subset of the data from the first H.E.S.S. publication on this source [11]. All observations were taken at an offset of 0.5 deg, at a zenith angle of 35-40 deg. The data set (see Figure 2.5) contains ~ 1500 gamma rays, with a significant signal from energy threshold at ~ 400 GeV up to ~ 10 TeV.

The motivation to include this source in the data release was to have a small extended source that allows morphology studies, i.e. measuring the source position, extension and elongation. There are other TeV sources in the field of view (HESS J1503-582, HESS J1457-593 and HESS J1458-608), but they are at an offset of more than one degree and fainter than MSH 15−52, so obtaining good results for MSH 15−52 is possible without modeling those other sources.
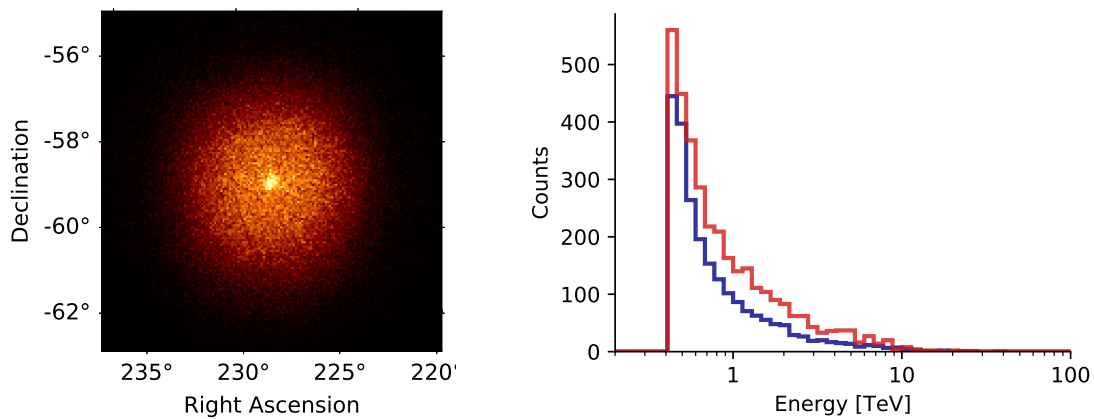

Figure 2.5: MSH 15−52 counts image (left) and counts spectrum (right) for a circular on region (total in red, background estimate using ring method in blue).

2.5   RX J1713.7−3946

The supernova remnant RX J1713.7−3946 is one of the largest (~ 1 deg diameter) and brightest TeV sources. It was selected for this data release as an example of a very extended source with a complex morphology. As shown in previous H.E.S.S. publications ([13], [14], [15]), gamma-ray emission is found all throughout the shell-type supernova remnant, at varying levels of intensity.

   This data release contains 7.0 hours of observation (15 runs) of RX J1713.7−3946 from 2004, a subset of the data used in early H.E.S.S. publications on this source ([13], [14]). Most observations were taken at an offset of 0.7 deg from the center of the SNR (three observations were pointing at the SNR center), at a zenith angle of 16-26 deg. The data set (see Figure 2.6) contains ~ 3600 gamma rays, with a significant signal from energy threshold at ~ 250 GeV up to ~ 10 TeV.
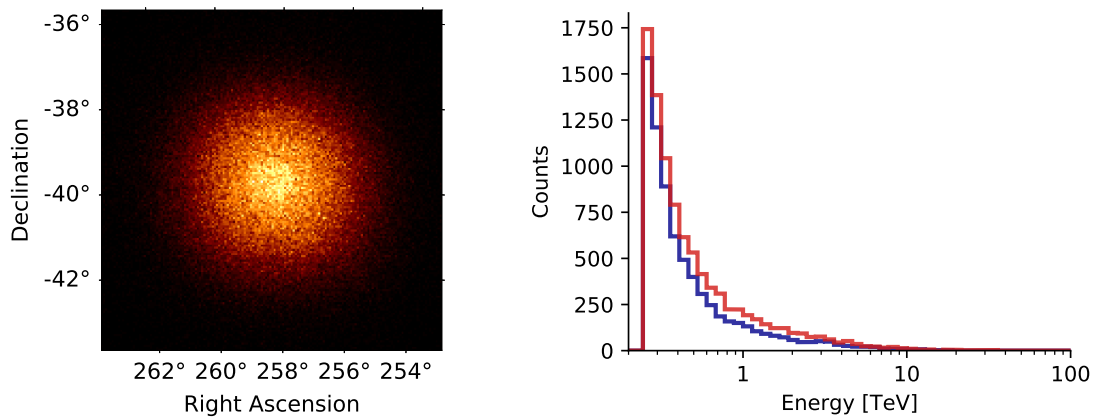

Figure 2.6: RX J1713.7−3946 counts image (left) and counts spectrum (right) for a circular on region (total in red, background estimate using ring method in blue).

2.6 Off runs

Modeling the gamma-like hadronic background is perhaps the most difficult aspect for many IACT data analyses. Background is usually estimated from real data (not Monte-Carlo simulations), either from the mostly empty parts within the field of view of a given run, or from other so called "off" observations of mostly empty fields of view [18, 19]. For the H.E.S.S. experiment there exists an "off run list" consisting mostly of observations that did not result in a detection (and a small fraction of dedicated off observations), that is used in H.E.S.S. to construct background models (usually by grouping in zenith angle bins).

Here we release a very small subset of 20.7 hours (45 runs) of the H.E.S.S.-internal "off run list" that contains thousands of runs. It can be used as a small example dataset to study H.E.S.S. background, or to develop codes and methods to create background models. However, we note that this is limited due to the small size of this dataset, e.g. template background models that represent the spatial shape and / or spectrum will be noisy due to the small number of events available.

3. Data files

3.1 Overview

The release notes document `hess_dl3_dr1.pdf` (the one you are reading at the moment) is available as a separate file from the data release webpage.

The data from this release is contained in a gzipped tarball with filename `hess_dl3_dr1.tar.gz`. To extract the content of the tarball, the following commmand can be used:

```
tar zxf hess_dl3_dr1.tar.gz
```

This will result in a directory called `hess_dl3_dr1` with the sub-directories and files shown in Figure 3.1 on the next page. The total size of the files in this data release is 42.8 MB.

The `README.txt` file contains a brief description of the data release, as well as the terms of use.

The rest of the files are gzipped FITS files. FITS is a standard data exchange and archival format in astronomy. It supports the storage of multiple header data units (HDUs) in one FITS file. We store all data in binary table (BINTABLE) HDUs.

The observation index table in `obs-index.fits.gz` and HDU index table in `hdu-index.fits.gz` can be used to select and load data, they are described in Section 3.2.

The data for each observation run is contained in a single FITS with name `hess_dl3_dr1_obs_id_NNNNNN.fits.gz`, where `NNNNNN` is the `OBS_ID` number of the run. For each run there are five HDUs (names: `EVENTS`, `GTI`, `AEFF`, `EDISP` and `PSF`) that are summarised in Table 3.1 and described in the remaining sections of this chapter.

A detailed data format specification is available separately in the "Data formats for gamma-ray astronomy" document version 0.2, which is available on Github[1], Readthedocs[2] and archived on Zenodo [20]. This chapter only describes additional information that is specific to this H.E.S.S. data release, such as e.g. which IRF formats we use and what axis binnings. Further information on how this DL3 FITS data was produced, as well as notes and caveats concerning the IRFs, is given in Section 4.1.

---

[1]`https://github.com/open-gamma-ray-astro/gamma-astro-data-formats`
[2]`https://gamma-astro-data-formats.readthedocs.io/`

```
├── hess_dl3_dr1.pdf

├── hess_dl3_dr1.tar.gz

├── hess_dl3_dr1

    ├── README.txt

    ├── hdu-index.fits.gz

    ├── obs-index.fits.gz

    ├── data

        ├── hess_dl3_dr1_obs_id_NNNNNN.fits.gz

        ├── hess_dl3_dr1_obs_id_NNNNNN.fits.gz

        ├── ...
```
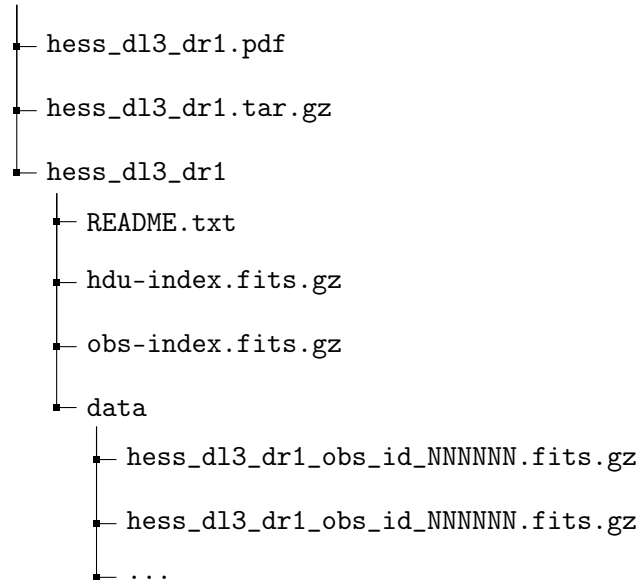
Figure 3.1: Directory structure and files in the release tarball. The `hess_dl3_dr1.pdf` and `hess_dl3_dr1.tar.gz` files are part of the data release. After downloading and extracting `hess_dl3_dr1.tar.gz` via `tar xvf hess_dl3_dr1.tar.gz` you will find the `hess_dl3_dr1` folder and files as shown.

HDU	Description	HDUCLAS4	Rows	Cols	Size (kB)
EVENTS	Event parameters		9,963	5	360.1
GTI	Good time intervals		2	2	5.6
AEFF	Effective area	AEFF_2D	1	5	11.2
EDISP	Energy dispersion	EDISP_2D	1	7	368.4
PSF	Point spread function	PSF_TABLE	1	7	115.3

Table 3.1: FITS HDU overview. All HDUs are BINTABLE HDUs, all IRFs are full-enclosure IRFs. Mean HDU size is given in kilo-bytes (kB). Number of rows for EVENTS is the average, for the other tables it is always the same.

3.2 Index files

The observation index table in `obs-index.fits.gz` and HDU index table in `hdu-index.fits.gz` can be used to select and load data. Their format is described in the open specifications. We note that using these index files is optional, with a small effort to select runs and declare the input data correctly, it is possible to access and load the data with Gammapy or ctools without using these index files.

The observation index table in `obs-index.fits.gz` has 105 rows, one row per observation run. The 31 columns list the parameters that can be useful for run selection. The `OBS_ID` identifies the observation, and e.g. the `RA_PNT` and `DEC_PNT` columns give the run pointing position. All of the information shown in the Tables 2.1, 2.2, A.2 and in Figure 2.1 is contained in the observation index table. Most of the parameters for a given observation are also contained in the `EVENTS` FITS header under the same key name. A few more columns have been added for convenience, e.g. the `SAFE_ENERGY_LO` in the observation table is taken from the `LO_THRES` key in the `AEFF` FITS header. The `TARGET_NAME` key was added that gives the observation subset name shown in Table 2.2; this is the easiest way to select e.g. all "PKS 2155-304 (flare)" or all "Off data" runs in this data release.

The HDU index table in `hdu-index.fits.gz` can be used to locate and load any FITS HDU. It has 5×105 rows (one for each of the 5 different HDUs and each observation run) and 7 columns that give the type, size and location of each HDU, i.e. the folder relative to the index file, the filename and the HDU name.

3.3 Events

The H.E.S.S. data is given as an event list in a FITS HDU called `EVENTS` for each observation, with columns `EVENT_ID`, `TIME`, `RA`, `DEC` and `ENERGY`.

The H.E.S.S. observatory location (usually not needed for science analysis) is:

```
GEOLAT  =     -23.2717777777778 / latitude of observatory (deg)
GEOLON  =      16.5002222222222 / longitude of observatory (deg)
ALTITUDE=                 1835. / altitude of observatory (m)
```

The H.E.S.S. reference time is defined following the FITS time standard, with the following values:

```
MJDREFI =                 51910 / int part of reference MJD for times
MJDREFF = 0.000742870370370241 / fractional part of MJDREF
TIMEUNIT= 's       '            / time unit is seconds since MET start
TIMESYS = 'TT      '            / Time system (TT=terrestrial time)
TIMEREF = 'local   '            / local time reference
```

In H.E.S.S., there is no unique EVENT ID. Instead, there are two numbers that together uniquely identify an event within a given `OBS_ID`, the so-called bunch number (the result of how data acquisition works in H.E.S.S.) and event number within a bunch. To comply with the DL3 spec, which requires a unique `EVENT_ID` within a given `OBS_ID`, we have decided to fill `EVENT_ID` as follows in the H.E.S.S. FITS exporters:

```
EVENT_ID = (BUNCH_ID_HESS << 32) | (EVENT_ID_HESS)
```

3.4 Good time intervals

The good time interval table `GTI` is something that is commonly used in high-energy missions since decades to declare the observation times corresponding to the given events. For this H.E.S.S. data we give it as well, even though the GTI tables always consist of a single row giving the start and stop time for each observation. The same information is already present in the header of the `EVENTS` extension under the `TSTART` and `TSTOP` keys, and in addition in a timestamp string format via the `DATE-OBS` and `TIME-OBS` (start) and `DATE-END` and `TIME-END` (stop) keys. To compute exposures and fluxes from the data released here, the `LIVETIME` header key in the `EVENTS` HDU can be accessed, or equivalently, the `ONTIME` and dead time correction factor `DEADC` from there could be used, since

```
ONTIME = TSTOP - TSTART
LIVETIME = DEADC x ONTIME
```

3.5 Instrument responses

This section contains general comments on the instrument response function (IRF) information that is described in the following sections. For every observation we assume that the instrument response function (IRF) is stable. This is an approximation, in reality there is a small variation in response, mainly because of the zenith angle variation during the run.

The response is stored in FITS HDUs, for the following quantities:
- **aeff**: Effective area in `aeff_2d` format. See Section 3.6.
- **edisp**: Energy dispersion in `edisp_2d` format. See Section 3.7.
- **psf**: Point spread function in `psf_table` format. See Section 3.8.

We note that the MC statistics for the IRFs used here is high, even at high energies. The Poisson noise and re-sampling artifacts are relatively low, and the dependence of IRFs on parameters like energy or offset is usually smooth. In practice this means that science tools can directly use the IRFs using linear interpolation or even nearest-bin queries and obtain good results.

That said, we note that no quantitative IRF error is given. When analyzing this data, please note the following caveats:
- Some instrumental effects (e.g. broken pixels in the camera images) are known to broaden the gamma-ray PSF, yet are not taken into account in the MC point-source simulations here. No evaluation of the PSF systematics and precision is given for this PSF.
- The assumed IRFs in the data release are computed for the mean zenith angle during the run, where in reality the zenith angle varies somewhat during the run and across the field of view.
- Similarly, IRFs are computed from point-source simulations at fixed zenith, azimuth and field-of-view offset angles, so for any given source position some interpolation error results. This can be a problem in particular close to the energy threshold, which is a function of, e.g., the zenith angle.
- The offset binning has been chosen to reflect the H.E.S.S. simulation of IRFs, which is carried out at six different offset angles, namely 0.0, 0.5, 1.0, 1.5, 2.0, and 2.5 deg. Since the IRFs are computed using point-source simulations at fixed offsets, the bins are defined such that their low and high edges are identical, and equal to the offset angle that was simulated (e.g. the first bin has edges (0 deg, 0 deg)).

The IRF uncertainties translate into systematic errors on high-level analysis results. For previous H.E.S.S. publications, our knowledge of the whole instrumental chain, the uncertainties of the Monte Carlo simulations and of the analysis chain (calibration, reconstruction and discrimination) lead to an estimation of the systematic errors of 20% on the flux and 0.1 on the spectral index for a bright isolated point source [1], and up to 30% and 0.2 respectively or more for extended sources in the Galactic plane [21]. The systematic error of the reconstructed source location is less than 20 arcsec in RA and Dec [22]. For this FITS dataset, no evaluation of systematic errors has been performed yet.

3.6 Effective area

Effective areas are stored in the `aeff_2d` format and are illustrated in Figure 3.2.

The effective area IRF has two axes:
- The field of view offset axis has bins located at 0, 0.5, 1.0, 1.5, 2.0 and 2.5 deg. This is identical for all IRFs and explained in Section 4.1.2.
- The energy binning is equally spaced in the logarithm of the energy, with 96 bins from 0.01 TeV to 100 TeV (24 bins per decade in energy). This energy binning is fine enough so that there should be no effects due to interpolation performed by science tools when evaluating the data.

For technical reasons, the curves have been smoothed by fitting a high-degree polynomial function to the simulated histogram. This fit can sometimes diverge in the last few bins at the highest energies (due to missing simulation data at even higher energies). However, it has been verified that the fit is still in good agreement with the underlying histogram within its statistical uncertainties in all cases.
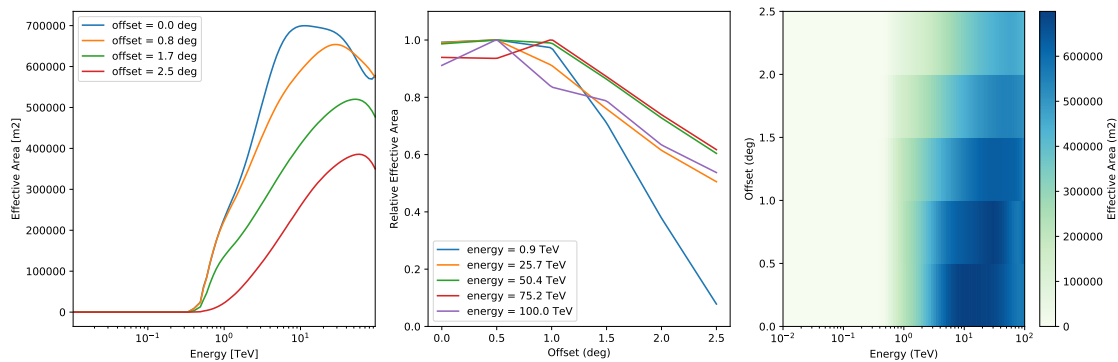
Figure 3.2: Effective area for observation `OBS_ID=23523` at the Crab nebula position (zenith angle 49 deg, FOV offset 0.5 deg, safe energy threshold 0.69 TeV).

3.7 Energy dispersion

Energy dispersion is stored in the `edisp_2d` format and is illustrated in Figure 3.3.

The energy dispersion IRF has three axes:
- The field of view offset axis has bins located at 0, 0.5, 1.0, 1.5, 2.0 and 2.5 deg. This is identical for all IRFs and explained in Section 4.1.2.
- The energy axis has 96 bins, logarithmically spaced between 0.01 TeV and 100 TeV.
- The `MIGRA` axis (defined as reconstructed over true energy ratio) has a linear binning with a bin width of 0.03, ranging from 0.2 and 5.0 (160 bins). This bin width of 3% energy resolution is good enough to capture the shape of the H.E.S.S. energy dispersion, which has a width of roughly 15%.
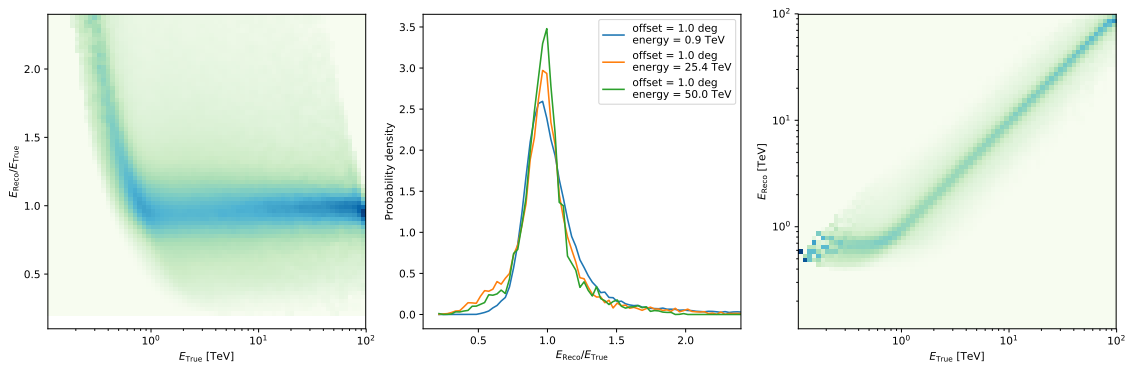
No smoothing was applied.

Figure 3.3: Energy dispersion for observation `OBS_ID=23523` at the Crab nebula position (zenith angle 49 deg, FOV offset 0.5 deg, safe energy threshold 0.69 TeV).

3.8 Point spread function

The point spread function is stored in the `psf_table` format and is illustrated in Figure 3.4. It is assumed to be radially symmetric.

The point spread function IRF has three axes:
- The field of view offset axis has bins located at 0, 0.5, 1.0, 1.5, 2.0 and 2.5 deg. This is identical for all IRFs and explained in Section 4.1.2.
- The energy binning is equally spaced in the logarithm of the energy, with 32 bins from 0.01 TeV to 100 TeV.
- The binning of the radial parameter `RAD` of the point spread function is equally spaced in angle-squared up to 0.1 deg. Further bins are equally spaced in square-root of the angle. The PSF is stored for radial offsets from 0 deg to 0.67 deg in the file (144 bins in total).

This binning in `RAD` has been chosen in order to preserve all information about the shape of the point spread function in its core region that is available from the simulated H.E.S.S. IRF. At positions further away from the core the binning can be more coarse because the point spread function changes very slowly with increasing distance to the core.
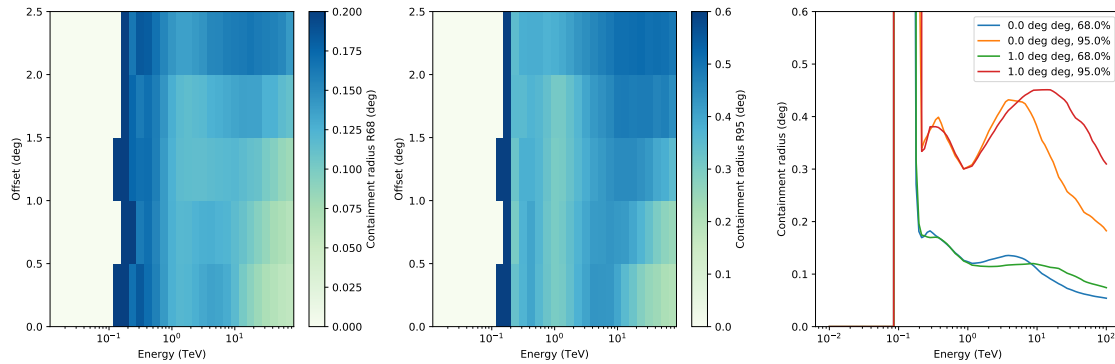
No smoothing was applied.

Figure 3.4: Point spread function for observation `OBS_ID=23523` at the Crab nebula position (zenith angle 49 deg, FOV offset 0.5 deg, safe energy threshold 0.69 TeV).

4. Notes

This section contains additional notes: Section 4.1 describes in detail how these FITS data were produced, mostly focused on information and caveats for the instrument response functions. Section 4.2 gives information how to analyse this data.

4.1 H.E.S.S. DL3 FITS production

This section contains detailed information about how the DL3 data were produced.

It comprises software and version numbers, but also general information on data calibration, event reconstruction, gamma-hadron separation and IRF production that are important to explain the features visible in the event parameter distributions or IRFs.

4.1.1 Overview

To produce DL3 data, the following main steps are performed: calibration, event reconstruction, gamma-hadron separation, data quality selection. For this data release we decided to use what is known in H.E.S.S. as "Heidelberg calibration", event stereo "Hillas reconstruction", "standard cuts" with full enclosure effective areas and "spectral data quality selection". This is described in detail in the "Observations of the Crab nebula with H.E.S.S." paper from 2006 [1]. All data was taken with the H.E.S.S. I array, with all 4 telescopes participating in each observation, and at least two telescopes triggering for each event.

We would like to note that Hillas reconstruction and standard cuts do not represent the state of the art for H.E.S.S. analysis. All recent and ongoing H.E.S.S. publications use better, more sensitive methods, e.g. multivariate gamma-hadron separation such as [23] or [24] or air shower template-based event reconstruction such as [25] or [26]. As stated in Section 1.2, the goal of this data release is to test data models, formats and science tools, not to offer the most sensitive H.E.S.S. analysis. The main reason we chose Hillas standard cuts is that the data and IRFs are stable (updated last in 2011), well-tested and robust. The more modern analyses with better background rejection and sensitivity typically are less stable (e.g. with respect to small calibration issues), and exhibit features that complicate the analysis, such as steps in energy for effective area and event distributions due to training of gamma-hadron separation in energy bands.

This FITS dataset was produced using DST version 12-03, and the HAP analysis configuration `std_fullEnclosure_fits_release`. The software used was the `hess-data-fits-export` batch script, which calls `hap` to export the `EVENT` data and `hap-to-irf` to export the IRFs, using the software version as of May 6, 2018. The script used Astropy 3.1 and Gammapy 0.8 to process and check the data.

4.1.2 IRFs

The effective area, energy dispersion and PSF IRFs were computed from point-source Monte Carlo (MC) simulations with a power-law energy spectrum (spectral index -2) and a grid of values in the following parameters:

- Zenith angles: 0, 10, 20, 30, 40, 45, 50, 55, 60, 63, 65 deg
- Offset angles: 0.0, 0.5, 1.0, 1.5, 2.0, 2.5 deg
- Azimuth angles: 0, 180 deg (north and south)
- Muon efficiency configs: 100, 101, 102, 103, 104, 105

The muon efficiency configurations correspond to different intervals in time with varying optical efficiency of the telescopes. Their labels are arbitrary and carry no physical information.

The IRFs for a given run were computed by interpolating between these parameters / configurations. For the pointing position, the average zenith and azimuth angles of the events recorded during the observation were used. The H.E.S.S. lookup production, and the computation of "effective" IRFs for a given run as performed here, are complicated in detail, and described in the H.E.S.S.-internal note [27].

4.2   Analysis recommendations

This section contains some information how to analyse the data presented here.

4.2.1 Tools

The data in this release are in a standard, well-documented format (for its definition, see `https://gamma-astro-data-formats.readthedocs.io/` and [3]). At the time of this data release, this format is supported by two open-source science tool packages: Gammapy (see `http://gammapy.org/`and [4, 5]), currently at version 0.8 and ctools (see `http://cta.irap.omp.eu/ctools/`and [6]), currently at version 1.5.

We do not give any tutorial or present any results here for the analysis of this data. A future publication with a detailed analysis and comparison of H.E.S.S. data with the internal tools, Gammapy and ctools is in preparation. Tutorials for Gammapy or ctools or other science tool packages analysing this data are very welcome, but will be left to the science tool teams to create and maintain.

4.2.2 Safe cuts

When analysing these data, it is recommended to apply a safe energy and maximum field of view (FOV) cut.

The `AEFF_2D` table includes a keyword `LO_THRESH`, which denotes the lower "safe" energy threshold for the observation. The threshold was computed as the energy at which the energy bias equals 10%, at an offset of 1 degree in the field of view. Figure 2.1 shows the distribution of "safe" energy threshold values for the observation runs in this data release. It varies between 200 GeV and 1 TeV. Higher zenith-angle runs have a larger energy threshold, and to a lesser degree also later runs have a higher energy threshold, because the optical efficiency of the telescopes decreases over time.

For analyses based on these H.E.S.S. data, we recommended to apply a minimum energy cut matching this safe energy threshold when performing an analysis, because the responses at lower

energies are unreliable (all of them: effective area, energy dispersion and point spread function).

It is also recommended to apply a maximum field of view offset cut of 2 degrees, because at larger offsets the responses are unreliable.

4.2.3 Background modeling

This data release does not contain background models. To analyse it, we recommend you use background modeling techniques that estimate the background from the event data such as the reflected background method to derive spectra or the ring background method without an offset acceptance correction, or use the off run data given to estimate the background via the on-off method, or by generating a background template model from the off runs. A good reference for background estimation methods in VHE gamma-ray astronomy is [18].

5. Acknowledgements

References

[1]   F. Aharonian et al. "Observations of the Crab nebula with HESS". In: *AAP* 457 (Oct. 2006), pages 899–915. DOI: 10.1051/0004-6361:20065351. eprint: arXiv:astro-ph/0607333 (cited on pages 1, 4, 6, 15, 19).

[2]   W. D. Pence et al. "Definition of the Flexible Image Transport System (FITS), version 3.0". In: *AAP* 524 (Dec. 2010), A42+. DOI: 10.1051/0004-6361/201015362 (cited on page 1).

[3]   C. Deil et al. "Open high-level data formats and software for gamma-ray astronomy". In: *ArXiv e-prints* (Oct. 2016). arXiv: 1610.01884 [astro-ph.IM] (cited on pages 2, 20).

[4]   A. Donath et al. "Gammapy - A Python package for gamma-ray astronomy". In: *ArXiv e-prints* (Sept. 2015). arXiv: 1509.07408 [astro-ph.IM] (cited on pages 2, 20, 23).

[5]   C. Deil et al. "Gammapy - A prototype for the CTA science tools". In: *ArXiv e-prints* (Sept. 2017). arXiv: 1709.01751 [astro-ph.IM] (cited on pages 2, 20, 23).

[6]   J. Knödlseder et al. "GammaLib and ctools. A software framework for the analysis of astronomical gamma-ray data". In: *AAP* 593, A1 (Aug. 2016), A1. DOI: 10.1051/0004-6361/201628822. arXiv: 1606.00393 [astro-ph.IM] (cited on pages 2, 20).

[7]   M. Holler et al. "Advanced search for the extension of unresolved TeV sources with H.E.S.S.: First measurement of the extension of the Crab nebula at TeV energies". In: *ArXiv e-prints* (July 2017). arXiv: 1707.04196 [astro-ph.HE] (cited on pages 4, 6).

[8]   F. Aharonian et al. "Simultaneous Observations of PKS 2155-304 with HESS, Fermi, RXTE, and Atom: Spectral Energy Distributions and Variability in a Low State". In: *APJL* 696 (May 2009), pages L150–L155. DOI: 10.1088/0004-637X/696/2/L150. arXiv: 0903.2924 [astro-ph.HE] (cited on pages 4, 7).

[9]   F. Aharonian et al. "Simultaneous multiwavelength observations of the second exceptional γ-ray flare of PKS 2155-304 in July 2006". In: *AAP* 502 (Aug. 2009), pages 749–770. DOI: 10.1051/0004-6361/200912128. arXiv: 0906.2002 (cited on pages 4, 7).

[10] H.E.S.S. Collaboration et al. "A multiwavelength view of the flaring state of PKS 2155-304 in 2006". In: *AAP* 539, A149 (Mar. 2012), A149. DOI: 10.1051/0004-6361/201117509. arXiv: 1201.4135 [astro-ph.HE] (cited on pages 4, 7).

[11] F. Aharonian et al. "Discovery of extended VHE gamma-ray emission from the asymmetric pulsar wind nebula in MSH 15-52 with HESS". In: *AAP* 435 (May 2005), pages L17–L20. DOI: 10.1051/0004-6361:200500105. eprint: arXiv:astro-ph/0504120 (cited on pages 4, 8).

[12] M. Tsirou et al. "VHE gamma-ray study of the composite SNR MSH 15-52 with H.E.S.S". In: *ArXiv e-prints* (Sept. 2017). arXiv: 1709.01422 [astro-ph.HE] (cited on pages 4, 8).

[13] F. Aharonian et al. "A detailed spectral and morphological study of the gamma-ray supernova remnant RX J1713.7-3946 with HESS". In: *AAP* 449 (Apr. 2006), pages 223–242. DOI: 10.1051/0004-6361:20054279. eprint: arXiv:astro-ph/0511678 (cited on pages 4, 9).

[14] F. Aharonian et al. "Primary particle acceleration above 100 TeV in the shell-type supernova remnant RX J1713.7-3946 with deep HESS observations". In: *AAP* 464 (Mar. 2007), pages 235–243. DOI: 10.1051/0004-6361:20066381. eprint: arXiv:astro-ph/0611813 (cited on pages 4, 9).

[15] H. E. S. S. Collaboration et al. "H.E.S.S. observations of RX J1713.7-3946 with improved angular and spectral resolution; evidence for gamma-ray emission extending beyond the X-ray emitting shell". In: *ArXiv e-prints* (Sept. 2016). arXiv: 1609.08671 [astro-ph.HE] (cited on pages 4, 9).

[16] T.-P. Li and Y.-Q. Ma. "Analysis methods for results in gamma-ray astronomy". In: *APJ* 272 (Sept. 1983), pages 317–324. DOI: 10.1086/161295 (cited on page 4).

[17] E. Aliu et al. "Observation of Pulsed γ-Rays Above 25 GeV from the Crab Pulsar with MAGIC". In: *Science* 322 (Nov. 2008), pages 1221–. DOI: 10.1126/science.1164718. arXiv: 0809.2998 (cited on page 6).

[18] D. Berge, S. Funk, and J. Hinton. "Background modelling in very-high-energy γ-ray astronomy". In: *AAP* 466 (May 2007), pages 1219–1229. DOI: 10.1051/0004-6361:20066674. eprint: arXiv:astro-ph/0610959 (cited on pages 10, 21).

[19] M. V. Fernandes et al. "A new method of reconstructing VHE γ-ray spectra: the Template Background Spectrum". In: *AAP* 568, A117 (Aug. 2014), A117. DOI: 10.1051/0004-6361/201323156. arXiv: 1407.0925 [astro-ph.IM] (cited on page 10).

[20] Christoph Deil et al. *Data formats for gamma-ray astronomy - version 0.2*. Sept. 2018. DOI: 10.5281/zenodo.1409831. URL: https://doi.org/10.5281/zenodo.1409831 (cited on page 11).

[21] H. E. S. S. Collaboration et al. "The H.E.S.S. Galactic plane survey". In: *AAP* 612, A1 (Apr. 2018), A1. DOI: 10.1051/0004-6361/201732098. arXiv: 1804.02432 [astro-ph.HE] (cited on page 15).

[22] Isabel Braun. "Improving the Pointing Precision of the H.E.S.S. Experiment". PhD thesis. Universität Heidelberg, Max-Planck-Institut für Kernphysik, May 2007 (cited on page 15).

[23] S. Ohm, C. van Eldik, and K. Egberts. "γ/hadron separation in very-high-energy γ-ray astronomy using a multivariate analysis method". In: *Astroparticle Physics* 31 (June 2009), pages 383–391. DOI: 10.1016/j.astropartphys.2009.04.001. arXiv: 0904.1136 (cited on page 19).

[24] Y. Becherini et al. "A new analysis strategy for detection of faint γ-ray sources with Imaging Atmospheric Cherenkov Telescopes". In: *Astroparticle Physics* 34 (July 2011), pages 858–870. DOI: 10.1016/j.astropartphys.2011.03.005. arXiv: 1104.5359 [astro-ph.HE] (cited on page 19).

[25] M. de Naurois and L. Rolland. "A high performance likelihood reconstruction of γ-rays for imaging atmospheric Cherenkov telescopes". In: *Astroparticle Physics* 32 (Dec. 2009), pages 231–252. DOI: 10.1016/j.astropartphys.2009.09.001. arXiv: 0907.2610 [astro-ph.IM] (cited on page 19).

[26] R. D. Parsons and J. A. Hinton. "A Monte Carlo template based analysis for air-Cherenkov arrays". In: *Astroparticle Physics* 56 (Apr. 2014), pages 26–34. DOI: 10.1016/j.astropartphys.2014.03.002. arXiv: 1403.2993 [astro-ph.IM] (cited on page 19).

[27] Henning Gast. *A new lookup scheme for hap*. HESS Internal Note. Mar. 2012 (cited on page 20).

[28] M. Wenger et al. "The SIMBAD astronomical database. The CDS reference database for astronomical objects". In: *AAPS* 143 (Apr. 2000), pages 9–22. DOI: 10.1051/aas:2000332. eprint: astro-ph/0002110 (cited on page 23).

[29] Astropy Collaboration et al. "Astropy: A community Python package for astronomy". In: *AAP* 558, A33 (Oct. 2013), A33. DOI: 10.1051/0004-6361/201322068 (cited on page 23).

[30] A. M. Price-Whelan et al. "The Astropy Project: Building an inclusive, open-science project and status of the v2.0 software". In: *ArXiv e-prints* (Jan. 2018). arXiv: 1801.02634 [astro-ph.IM] (cited on page 23).

A. Appendix

A.1 Acronyms

The following abbreviations are used throughout this document:

VHE   Very high energy (above $\sim$100 GeV)

DL3   Data level 3

GTI   Good time interval

FITS   Flexible Image Transport System

HDU   Header data unit of a FITS file

Run   Alternative term for "observation", commonly used for IACT data

IACT   Imaging atmospheric Cherenkov telescope

H.E.S.S.   High energy stereoscopic system

CTA   Cherenkov telescope array

PWN   Pulsar wind nebula

SNR   Supernova remnant

AGN   Active Galactic nucleus

MC   Monte Carlo

HAP   H.E.S.S. analysis program; one of the H.E.S.S.-internal analysis codes

FOV   Field of view

offset   Usually refers to offset in the field of view, i.e. with respect to the pointing position

IRF   Instrument response function

AEFF   Effective area

EDISP   Energy dispersion

PSF   Point spread function

OBS_ID   Observation identifier, a.k.a. run number

A.2 Full table of observations

Table A.1: Full table of observations. `OBS_ID` is the observation identifier (a.k.a. "run number"). `Duration` is the observation time (not deadtime corrected). The run pointing position is given in equatorial coordinates (`RA` and `DEC`) as well as Galactic coordinates (`GLON` and `GLAT`). `Offset` is the observation target object offset in the field of view, taken as `RA_OBJ` and `DEC_OBJ` from the FITS event list header, which is filled with the proposed target of observation from the H.E.S.S. database on FITS export. `Zenith` is the zenith angle of the observation at mid run time. A summary of the available observations grouped by sources is given in Table 2.2 on page 4.

OBS_ID	Date	Duration	RA	DEC	GLON	GLAT	Offset	Zenith
		min	deg	deg	deg	deg	deg	deg
Crab nebula observations (4 runs)								
23523	2004-12-04	28.1	83.6	21.5	185.0	−6.1	0.5	48
23526	2004-12-04	28.1	83.6	22.5	184.1	−5.5	0.5	45
23559	2004-12-06	28.1	85.3	22.0	185.4	−4.5	1.5	45
23592	2004-12-08	28.1	82.0	22.0	183.7	−7.0	1.5	48
PKS 2155−304 (flare) observations (15 runs)								
33787	2006-07-29	28.1	329.7	−29.7	18.5	−52.2	0.5	50
33788	2006-07-29	28.1	329.1	−30.2	17.6	−51.7	0.5	43
33789	2006-07-29	28.1	330.3	−30.2	17.8	−52.7	0.5	37
33790	2006-07-29	28.2	329.7	−30.7	16.9	−52.3	0.5	30
33791	2006-07-29	28.1	329.7	−29.7	18.5	−52.2	0.5	24
33792	2006-07-29	28.1	329.1	−30.2	17.6	−51.7	0.5	17
33793	2006-07-29	28.1	330.3	−30.2	17.8	−52.7	0.5	11
33794	2006-07-30	28.1	329.7	−30.7	16.9	−52.3	0.5	7
33795	2006-07-30	28.1	329.7	−29.7	18.5	−52.2	0.5	9
33796	2006-07-30	28.1	329.1	−30.2	17.6	−51.7	0.5	14
33797	2006-07-30	28.1	330.3	−30.2	17.8	−52.7	0.5	20
33798	2006-07-30	28.1	329.7	−30.7	16.9	−52.3	0.5	27
33799	2006-07-30	28.1	329.7	−29.7	18.5	−52.2	0.5	33
33800	2006-07-30	28.1	329.1	−30.2	17.6	−51.7	0.5	40
33801	2006-07-30	28.1	330.3	−30.2	17.8	−52.7	0.5	46
PKS 2155−304 (steady) observations (6 runs)								
47802	2008-08-27	28.1	330.3	−30.2	17.8	−52.7	0.5	36
47803	2008-08-27	28.1	329.1	−30.2	17.6	−51.7	0.5	30
47804	2008-08-27	28.1	329.7	−29.7	18.5	−52.2	0.5	23
47827	2008-08-28	28.1	330.3	−30.2	17.8	−52.7	0.5	35
47828	2008-08-28	28.1	329.1	−30.2	17.6	−51.7	0.5	29
47829	2008-08-28	28.1	329.7	−30.7	16.9	−52.3	0.5	22
MSH 15−52 observations (20 runs)								
20136	2004-03-26	28.0	228.6	−58.8	320.6	−0.9	0.4	38
20137	2004-03-26	15.0	228.6	−59.8	320.0	−1.7	0.6	40
20151	2004-03-27	28.1	228.6	−58.8	320.6	−0.9	0.4	37

Table A.1 – *Continued on next page*

Table A.1 – *Continued from previous page*

OBS_ID	Date	Duration	RA	DEC	GLON	GLAT	Offset	Zenith
		min	*deg*	*deg*	*deg*	*deg*	*deg*	*deg*
20282	2004-04-14	28.1	228.6	−58.8	320.6	−0.9	0.4	37
20283	2004-04-15	28.1	228.6	−59.8	320.0	−1.7	0.6	36
20301	2004-04-15	28.1	228.6	−58.8	320.6	−0.9	0.4	36
20302	2004-04-16	28.0	228.6	−59.8	320.0	−1.7	0.6	36
20303	2004-04-16	28.0	228.6	−58.8	320.6	−0.9	0.4	36
20322	2004-04-16	28.0	228.6	−59.8	320.0	−1.7	0.6	36
20323	2004-04-17	28.0	228.6	−58.8	320.6	−0.9	0.4	36
20324	2004-04-17	28.1	228.6	−59.8	320.0	−1.7	0.6	36
20325	2004-04-17	28.0	228.6	−58.8	320.6	−0.9	0.4	36
20343	2004-04-17	28.0	228.6	−58.8	320.6	−0.9	0.4	37
20344	2004-04-17	28.0	228.6	−59.8	320.0	−1.7	0.6	36
20345	2004-04-18	28.1	228.6	−58.8	320.6	−0.9	0.4	36
20346	2004-04-18	28.1	228.6	−59.8	320.0	−1.7	0.6	36
20365	2004-04-18	28.1	228.6	−59.8	320.0	−1.7	0.6	36
20366	2004-04-18	28.1	228.6	−58.8	320.6	−0.9	0.4	36
20367	2004-04-19	28.0	228.6	−59.8	320.0	−1.7	0.6	36
20368	2004-04-19	28.1	228.6	−58.8	320.6	−0.9	0.4	37

RX J1713.7−3946 observations (15 runs)

OBS_ID	Date	Duration	RA	DEC	GLON	GLAT	Offset	Zenith
20326	2004-04-17	28.1	259.3	−39.8	347.7	−1.0	0.7	18
20327	2004-04-17	28.1	257.5	−39.8	346.9	0.1	0.7	16
20349	2004-04-18	28.0	259.3	−39.8	347.7	−1.0	0.7	16
20350	2004-04-18	28.0	257.5	−39.8	346.9	0.1	0.7	18
20396	2004-04-20	28.1	258.4	−39.1	347.9	−0.1	0.7	16
20397	2004-04-20	28.0	258.4	−40.5	346.8	−0.9	0.7	19
20421	2004-04-21	28.1	258.4	−40.5	346.8	−0.9	0.7	16
20422	2004-04-21	28.1	258.4	−39.1	347.9	−0.1	0.7	19
20517	2004-04-24	28.1	257.5	−39.8	346.9	0.1	0.7	18
20518	2004-04-24	28.0	258.4	−39.1	347.9	−0.1	0.7	16
20519	2004-04-24	28.0	258.4	−40.5	346.8	−0.9	0.7	16
20521	2004-04-24	28.1	259.3	−39.8	347.7	−1.0	0.7	23
20898	2004-05-21	28.1	256.9	−40.5	346.1	0.0	1.3	26
20899	2004-05-21	28.0	257.5	−39.9	346.8	0.0	0.7	21
20900	2004-05-21	28.1	258.0	−39.3	347.5	0.0	0.5	18

Off data observations (45 runs)

OBS_ID	Date	Duration	RA	DEC	GLON	GLAT	Offset	Zenith
20275	2004-04-14	28.1	187.3	2.6	289.7	64.8	–	36
20339	2004-04-17	28.0	201.4	−42.3	309.6	20.1	–	24
20561	2004-04-26	28.1	232.4	−38.2	334.1	14.9	–	27
20734	2004-05-13	28.0	225.0	−41.9	327.1	14.8	–	37
20915	2004-05-22	28.0	186.8	2.1	288.8	64.3	–	29
21613	2004-07-15	28.0	349.8	−42.6	347.4	−65.7	–	21
21753	2004-07-21	28.0	349.8	−42.6	347.4	−65.7	–	19
21807	2004-07-24	28.0	343.7	−27.9	24.4	−64.2	–	9
21824	2004-07-25	28.0	356.4	−14.3	69.5	−70.0	–	9

Table A.1 – *Continued on next page*

Table A.1 – *Continued from previous page*

OBS_ID	Date	Duration	RA	DEC	GLON	GLAT	Offset	Zenith
		min	*deg*	*deg*	*deg*	*deg*	*deg*	*deg*
21851	2004-07-28	28.0	27.1	13.5	143.5	−47.0	–	42
22022	2004-08-13	20.0	255.7	−48.3	339.3	−4.0	–	43
22593	2004-09-20	28.1	80.0	−45.3	251.0	−34.6	–	39
22997	2004-10-11	28.1	40.2	−0.0	171.5	−52.3	–	24
23040	2004-10-14	28.1	68.6	−47.3	253.4	−42.5	–	24
23077	2004-10-15	28.1	40.2	−0.0	171.5	−52.3	–	29
23143	2004-10-21	28.1	88.3	−32.3	237.7	−25.7	–	23
23246	2004-11-07	28.1	67.8	5.4	190.1	−27.8	–	30
23573	2004-12-07	28.1	88.9	−38.6	244.7	−26.9	–	27
23635	2004-12-13	28.1	68.3	5.9	189.9	−27.1	–	32
23651	2004-12-14	28.1	68.3	4.9	190.8	−27.7	–	37
23736	2005-01-03	28.1	83.9	−69.8	280.3	−31.9	–	49
25345	2005-05-04	28.0	187.3	2.6	289.7	64.8	–	34
25443	2005-05-08	27.9	187.3	2.6	289.7	64.8	–	26
25511	2005-05-11	27.9	187.8	2.1	291.1	64.5	–	34
26077	2005-06-04	28.2	245.0	−14.9	359.7	24.2	–	41
26791	2005-06-27	20.7	233.7	24.2	37.8	53.2	–	52
26827	2005-06-29	28.2	234.5	23.5	36.9	52.4	–	46
26850	2005-06-30	28.2	263.4	−21.5	4.9	6.2	–	2
26964	2005-07-04	28.2	262.7	−20.8	5.1	7.2	–	12
27044	2005-07-07	28.2	262.7	−20.8	5.1	7.2	–	11
27121	2005-07-10	19.9	262.7	−22.2	3.9	6.4	–	2
27939	2005-08-12	28.2	355.9	−14.8	67.4	−70.0	–	9
27987	2005-08-13	28.2	54.6	−34.8	235.5	−53.6	–	21
28341	2005-08-31	28.2	310.0	−1.6	44.6	−24.8	–	23
28967	2005-09-30	28.2	310.0	−1.6	44.6	−24.8	–	23
28981	2005-10-01	28.2	56.7	1.1	186.4	−39.3	–	26
29024	2005-10-02	28.2	12.7	−25.3	117.4	−88.2	–	4
29072	2005-10-05	28.2	11.9	−26.0	85.4	−88.6	–	20
29118	2005-10-06	28.2	12.7	−25.3	117.4	−88.2	–	12
29177	2005-10-09	28.2	63.7	1.1	191.5	−33.6	–	26
29433	2005-10-24	28.2	9.0	−71.7	304.7	−45.4	–	50
29487	2005-11-02	28.2	11.9	−24.6	103.7	−87.3	–	3
29526	2005-11-04	28.2	7.3	−73.0	305.2	−44.0	–	52
29556	2005-11-06	28.2	64.2	0.6	192.3	−33.4	–	25
29683	2005-11-20	28.2	9.0	−71.7	304.7	−45.4	–	49